Intracellular Ca Alternans: Coordinated Regulation by Sarcoplasmic Reticulum Release, Uptake, and Leak

Lai-Hua Xie, Daisuke Sato, Alan Garfinkel, Zhilin Qu, and James N. Weiss
Cardiovascular Research Laboratory, Department of Medicine (Cardiology), David Geffen School of Medicine at the University of California, Los Angeles, California 90095

ABSTRACT Beat-to-beat alternation in the cardiac intracellular Ca (Ca_i) transient can drive action potential (AP) duration alternans, creating a highly arrhythmogenic substrate. Although a steep dependence of fractional sarcoplasmic reticulum (SR) Ca release on SR Ca load has been shown experimentally to promote Ca_i alternans, theoretical studies predict that other factors are also important. Here we present an iterated map analysis of the coordinated effects of SR Ca release, uptake, and leak on the onset of Ca_i alternans. Predictions were compared to numerical simulations using a physiologically realistic AP model as well as to AP clamp experiments in isolated patch-clamped rabbit ventricular myocytes exposed to 1), the Ca channel agonist BayK8644 (100 nM) to increase SR Ca load and release fraction, 2), overexpression of an adenoviral SERCA2a construct to increase SR Ca uptake, and 3), low-dose FK506 (20 μM) or ryanodine (1 μM) to increase SR Ca leak. Our findings show that SR Ca release, uptake, and leak all have independent direct effects that promote (release and leak) or suppress (uptake) Ca_i alternans. However, since each factor affects the other by altering SR Ca load, the net balance of their direct and indirect effects determines whether they promote or suppress alternans. Thus, BayK8644 promotes, whereas Ad-SERCA2a overexpression, ryanodine, and FK506 suppress, Ca_i alternans under AP clamp conditions.

INTRODUCTION

Recent evidence indicates that beat-to-beat alternation of the cardiac intracellular Ca (Ca_i) transient plays a key role in the development of action potential duration (APD) alternans (1–4). APD alternans can create a highly arrhythmogenic substrate, especially when it becomes spatially discordant, promoting conditions that favor reentry and fibrillation (5–9). Therefore, understanding the mechanisms causing Ca_i alternans, and the interaction with other factors contributing to APD alternans, is of considerable interest and may have clinical implications for the development of antiarrhythmic strategies.

Previous studies have documented that the Ca_i transient can alternate on a beat-to-beat basis even when the voltage waveform is fixed (1). Subsequent experimental and theoretical studies have demonstrated that alternans is promoted when the fraction of Ca released by the sarcoplasmic reticulum (SR) has a steep dependence on either SR Ca load (9–11) or, alternatively, on Ca-mediated refractoriness of SR release channels (12). The relationship between fractional SR Ca release and SR Ca load (hereafter referred to as SR Ca release slope) is highly nonlinear, rising steeply as SR Ca content increases (13,14); so alternans can be induced by conditions promoting high SR Ca loads such as rapid pacing (9,11,12) or interventions that increase the sensitivity of SR Ca release channels to Ca-induced Ca release (CICR) waves (10,15). A direct role of the SR Ca load controlling SR Ca release during Ca_i alternans, however, has been questioned, since a recent study demonstrated that Ca_i alternans can occur in the absence of detectable fluctuations in end-diastolic SR Ca load (12).

In addition to SR Ca release slope, theoretical analysis predicts that the rate of SR Ca uptake also has a prominent role in regulating the onset of Ca_i alternans, as illustrated schematically in Fig. 1. Shiferaw et al. (11) developed an iterated map approach to analyze formally how steep SR Ca release slope and SR Ca uptake rate coregulate the onset of Ca_i alternans, which they substantiated by numerical simulations in a dynamic cardiac Ca cycling model. A later study (16) further generalized their findings to the case in which total cellular Ca content was allowed to fluctuate during alternans. Consistent with these predictions, preliminary reports indicated that adenoviral overexpression of SERCA2a in isolated myocytes (17) suppressed APD and Ca_i alternans (without voltage control). To our knowledge, however, there is no direct experimental evidence showing how SR Ca uptake rate affects Ca_i alternans when the AP waveform is clamped.

Previous theoretical analyses of Ca_i alternans also have not taken into account the role of SR Ca leak. Repolarization alternans and pulsus alternans are common in the failing heart, in which increased SR Ca leak plays a pathophysiological role (18). In addition, genetically altered mice with increased SR leak due to FBP12.6 deficiency have been reported to have increased susceptibility to APD alternans (19).

Submitted February 7, 2008, and accepted for publication May 27, 2008.

Lai-Hua Xie and Daisuke Sato contributed equally to this work.

Address reprint requests to James N. Weiss, MD, Division of Cardiology, Rm. 3645 MRL Building, UCLA School of Medicine, Los Angeles, CA 90095. Tel.: 310-825-9029; Fax: 310-206-5777; E-mail: jweiss@mednet.ucla.edu.

Lai-Hua Xie's present address is the Dept. of Cell Biology and Molecular Medicine, University of Medicine and Dentistry of New Jersey-New Jersey Medical School, Newark, NJ 07103.

Editor: David A. Eisner.

0006-3495/08/09/3100/11 $2.00

doi: 10.1529/biophysj.108.130955

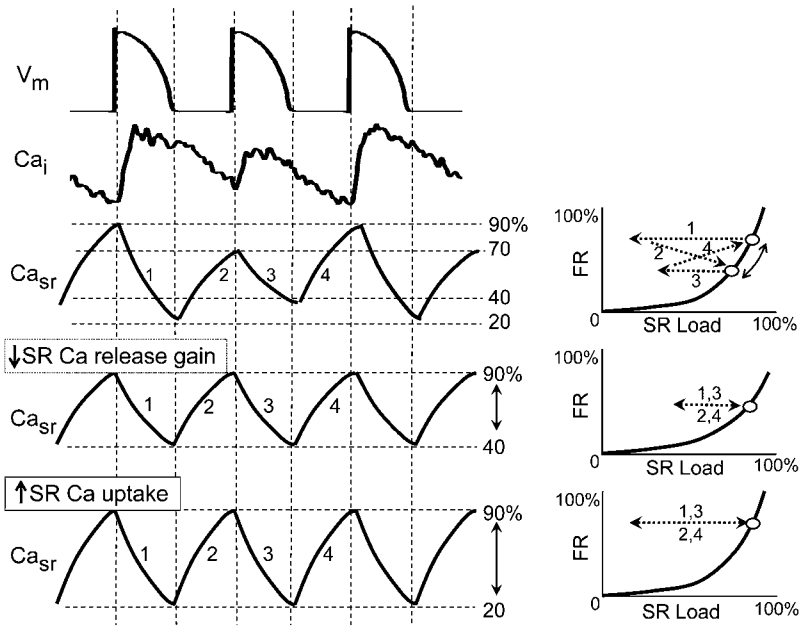

FIGURE 1 Illustration of how SR Ca release gain and uptake coregulate Ca_i alternans. The upper two traces show an AP clamp waveform (V_m) and the corresponding alternating Ca_i transient (Ca_i) recorded from a rabbit ventricular myocyte during pacing at 210 ms CL. The third tracing illustrates hypothetically how SR Ca content may be concomitantly alternating as a result of the steep nonlinear relationship between fractional release (FR) of SR Ca and SR Ca load shown in the graph at the right. Before the large Ca_i transient, the SR Ca load is high (90%), promoting a large FR (70%) that drains the SR to 20% (labeled step 1). If the SR Ca reuptake by SERCA2a can recover only 50% of the SR Ca store, then the SR load before the next beat will recover to only 70%. The lower SR load results in a reduced smaller Ca release (30%) on the next beat, draining the SR to 40% (step 3). However, now the 50% SR Ca reuptake can again restore the SR Ca load to 90% (step 4), causing a large (70%) release on the next beat, and so forth. The fourth panel illustrates conceptually how decreasing the slope of the SR release-load curve (i.e., decreasing m) abolishes alternans. At 90% SR Ca load, the reduced FR of only 50% now allows the same level of SERCA2a function to fully recover the SR load to 90% load before the next beat. The fifth panel illustrates conceptually how increasing SR Ca reuptake (u) for the same SR release-load curve abolishes alternans. At 90% SR Ca load, the FR is still 70%, but the enhanced SERCA2a function can now recover the full 70% instead of only 50%, restoring the SR Ca load to 90% before the next beat.

Whether increased SR Ca leak has any direct effect on Ca_i alternans, independent of its effects on SR Ca load/release, however, is unclear.

Accordingly, the objective of this work was to evaluate the contributions of SR Ca leak, uptake, and release on the genesis of Ca_i alternans in isolated cardiac myocytes using a combined theoretical, simulation, and experimental approach. We hypothesize that each factor has an independent effect on Ca_i alternans, such that their concerted interaction determines the threshold heart rate at which Ca_i alternans occurs. To test this hypothesis, theoretical predictions from an iterated map analysis were compared both to numerical simulations using a physiologically detailed action potential (AP) model (20) and to experimental findings in isolated rabbit ventricular myocytes before and after exposure to various interventions affecting different aspects of Ca_i cycling. To maximize physiological relevance, Ca_i alternans was induced by rapid pacing at physiological temperature using the perforated patch configuration to minimally disturb the intracellular milieu. We primarily used AP clamp conditions to avoid confounding influences of APD alternans on Ca_i alternans.

METHODS

Iterated map approach

The iterated map approach is based on formulating a set of equations summarizing how the values of key parameters on the current beat depend on their values from the previous beat, eliminating the need to integrate these parameters explicitly over time using detailed differential equations. This approach was first applied to the analysis of APD alternans by Nolasco and Dahlen (21) and subsequently extended to include Ca_i alternans (9,11,16). Here we extended these previous map models analyzing how SR Ca release and uptake affect the genesis of Ca alternans by adding the Ca leak into the map equations. The mathematical details are presented in the appendix.

In cardiac myocytes, contraction is activated by the process of CICR, in which a relatively small amount of Ca (10–30%) entering the cytoplasm through L-type Ca channels triggers the opening of SR Ca release channels (ryanodine receptors, RyR), releasing a larger amount of Ca stored in the SR (70–90%) into the cytoplasm (Fig. 1 *A*). RyR sensitivity to the triggering Ca is regulated by the free Ca concentration inside the SR lumen, which is proportional to the SR Ca load (Fig. 1 *B*). The goal of the iterated map formulation is to summarize how the Ca_i transient amplitude and SR Ca_i release, reuptake, and leak during the previous beat determine the values of the same parameters during the current beat. Unlike the classic iterated map analysis for APD alternans (21), in which a single parameter (APD restitution slope) controls alternans instability, the Ca_i-driven alternans map involves three parameters: m, the SR Ca release slope; u, the SR Ca uptake factor; and p, the SR Ca leak factor. Although u and p are formulated as phenomenological parameters rather than discrete biological entities, their values are intuitively related to the sensitivity of SR Ca uptake by SERCA2a to Ca_i and the sensitivity of SR Ca leak via RyR or other SR leak pathways to SR Ca load, respectively.

Computer simulation

Numerical simulations were performed using a recently developed rabbit ventricular AP model that was tuned to reproduce the APD restitution characteristics, APD alternans, and Ca_i dynamics measured experimentally in isolated rabbit ventricular myocytes (20). For control conditions, the maximum strength of uptake Ca flux was decreased from 0.4 μM/ms to 0.32 μM/ms, and the slope of the SR Ca release versus SR Ca load relationship at high loads was increased from 11.3 ms^{-1} to 13 ms^{-1}. These changes were made to match the pacing cycle length (CL) at the onset of Ca_i alternans in the

AP model to the average experimental value obtained from this set of isolated myocytes under the same conditions of pacing with an AP clamp waveform. To increase SR Ca release slope, we doubled the maximum conductance of the L-type Ca current $\bar{G}_{Ca}$, which also increased SR Ca load to a higher value of fractional SR Ca release. To increase SR Ca uptake, the maximum strength of uptake Ca flux v_{up} was increased by a factor of two. To increase SR Ca leak, the maximum strength of leak Ca flux g_l was increased by a factor of 20. The ordinary differential equations were numerically solved using the Euler forward method with a variable time step of 0.1 ~ 0.01 ms.

AP clamp

A single cell myocyte was paced using a clamped AP wave form as follows:

$$V(t) = \begin{cases} V_{min} + (V_{max} - V_{min})\sqrt{1 - \left(\dfrac{t - nT}{APD/T^2}\right)^2} & nT \le t \le nT + APD/T^2 \\ V_{min} & nT + APD/T^2 < t < (n+1)T \end{cases},$$

where $V_{max} = 0$ mV, $V_{min} = -80$ mV, T is the pacing CL, and n is the beat number. The APD was set to 200 ms. We used the identical pacing protocols as in the myocyte experiments (see below).

Calculation of iterated map parameters

For each of the above conditions, the map parameters m, p, and u (see Results) were calculated by pacing the cell model with a clamped AP waveform. The total Ca released by the SR (R) during the nth beat was calculated as

$$R_n = \int_{T_n}^{T_{n+1}} J_{rel}(t)dt,$$

where T_n is the beginning time of the nth beat. Similarly, the total amount of the SR Ca uptake (U) was calculated as

$$U_n = \int_{T_n}^{T_{n+1}} J_{up}(t)dt,$$

and the total amount of the SR leak (L) was calculated as

$$L_n = \int_{T_n}^{T_{n+1}} J_{leak}(t)dt.$$

The formulations of J_{rel}, J_{up}, and J_{leakl} are detailed in Mahajan et al. (20).

The SR Ca release slope m was then measured by perturbing the junctional SR Ca concentration c_j by 1–5% and measuring the effect on SR Ca release during the next beat using the following equation:

$$m = \frac{R_n - R_{n-1}}{c_n^{SR} - c_{n-1}^{SR}},$$

where c_n^{SR} is the diastolic Ca SR content at T_n. The SR Ca uptake factor u was calculated as

$$u = \frac{U_n - U_{n-1}}{c_n^{Cyto} - c_{n-1}^{Cyto}},$$

where c_n^{Cyto} is the peak Ca in the cytoplasm. The SR Ca leak factor p was calculated as

$$p = \frac{L_n - L_{n-1}}{c_n^{SR} - c_{n-1}^{SR}}$$

Myocyte experiments

Cell isolation

Ventricular myocytes were enzymatically isolated from adult rabbit hearts as described previously (22). Briefly, hearts were removed from adult New Zealand white rabbits (2–3 kg), anesthetized with intravenous pentobarbital, and perfused retrogradely in Langendorff fashion at 37°C with nominally Ca-free Tyrode's solution containing ~1.4 mg/ml collagenase (type II; Worthington, Lakewood, NJ) and 0.1 mg/ml protease (type XIV; Sigma, St. Louis, MO) for 25–30 min. After washing out the enzyme solution, the hearts were removed from the perfusion apparatus and swirled in a culture dish. The Ca concentration was slowly increased to 1.8 mM, and the cells were stored at room temperature and used within 8 h. This procedure typically yielded ~50% rod-shaped Ca-tolerant myocytes.

Adenoviral overexpression of SERCA2a

Myocytes in suspension were centrifuged for 3 min at 250 rpm and 25°C. After removing the supernatant and resuspending in Dulbecco's modified eagle medium (DMEM) with 1% penicillin/streptomycin two or three times, the cells were plated in 1 ml aliquots (average density of ~200,000 cells/ml) on 60 mm petri dishes containing 4 ml medium (DMEM: M199 = 4:1, P/S 1%, fetal bovine serum 10%) and incubated in 5% CO_2 at 37°C. Cells were precultured for 4–6 h before adding a SERCA2a-adenovirus construct (~10^{10}–10^{11} particles/ml) to achieve a multiplicity of transfectivity (MOI) of ~10 (8 μl in 4 ml medium). Robust gene expression with transfection rates of ~85–95%, as monitored by green fluorescent protein (GFP) fluorescence, was typically observed after 20–48 h. As a control, myocytes were transfected with adenovirus encoding for GFP alone using the same protocol.

Intracellular Ca measurement

Myocytes were loaded with the Ca indicator Fluo-4 by incubating them for ~30 min in bath solution containing 4 μM Fluo-4 AM or Rhod-2AM (Molecular Probes, Eugene, OR) and 0.016% (wt/wt) pluronic (Molecular Probes), after which the cells were washed and placed in a heated chamber on an inverted microscope. Ca_i fluorescence was recorded using an Andor Ixon charge-coupled device (CCD) camera (Andor Technology, South Windsor, CT) operating at ~100 frames per s with a spatial resolution of 512 × 180 pixels. Some data were obtained with a CCD camera (Model LCL 902K, Watec America, Orangeburg, NY), using an ATI video capture card (ATI Technologies, Sunnyvale, CA) (25 frames/s). The fluorescence intensity was measured in arbitrary units.

Patch-clamp methods

Myocytes were patch-clamped using the perforated patch whole cell recording mode. Patch pipettes (resistance 1–2 MΩ were dipped for ~10 s into the standard pipette solution containing (in mM) 110 KOH, 30 KCl, 5 NaCl, 10 HEPES, 1 EGTA, pH 7.2 with aspartic acid. EGTA was included to monitor if the cells were ideally perforated by observing cell contraction. The pipette was then back-filled using the same solution containing 240 μg/ml amphotericin-B (Sigma), as described by Rae et al. (23). The standard Tyrode's bath solution contained (in mM) 136 NaCl, 5.4 KCl, 0.33 Na_2PO_4, 1.8 $CaCl_2$, 1 $MgCl_2$, 10 glucose, and 10 HEPES, pH 7.4 adjusted with NaOH. In some experiments, BayK8644 (BayK, 100 nM), FK506 (20 μM),

and ryanodine (1 μM) were added directly to the bath superfusate. All experiments were performed at 34°C–36°C.

Membrane current and voltage were measured with an Axopatch 200B patch-clamp amplifier controlled by a personal computer using a Digidata 1200 acquisition board driven by pCLAMP 8.0 software (Axon Instruments, Foster City, CA). Most patch-clamp experiments were performed in the voltage clamp mode, using an AP waveform to pace the myocyte. Some experiments were also performed in the current clamp mode to record free-running APs during pacing protocols.

Pacing protocol

For AP clamp experiments, a previously recorded typical AP (APD_{90} of ~150 ms) was used as the voltage clamp waveform. During the pacing protocol, the initial pacing CL was set at 400 ms (or 450 ms for some BayK experiments) and decremented every 12 beats by 20 ms (from 400 to 300 ms), 10 ms (from 300 to 200 ms), or 5 ms (from 200 to 150 ms). The voltage file was recorded as a sound (.wav) file and played back to the Axon Digidata 1200 interface though a sound card with a Dell Optiplex GX 620 personal computer (Dell, Round Rock, TX). In current clamp experiments, free-running APs were recorded during the identical pacing sequence.

Data analysis

Data are presented as mean ± SE. Statistically significance was assessed using unpaired Student's *t*-tests or Fischer's exact test, with $p < 0.05$ considered significant.

RESULTS

Iterated map formulation of Ca_i cycling

As described in Methods, the iterated map formulation summarizes how the Ca_i transient amplitude and SR Ca_i release, reuptake, and leak during the previous beat determine the values of the same parameters during the current beat. The map analysis reveals that the threshold for Ca_i alternans is jointly regulated by SR release slope m, SR Ca uptake factor u, and SR Ca leak factor p according to the following equation:

$$(m + p - 1)(1 - u) > 1,$$

as illustrated graphically in Fig. 2. The three colored lines, corresponding to different values of SR Ca leak p, separate the region of alternans (above the lines) from the regions of no alternans (below the lines) in m-u phase space. The notable features are the following: 1), a steeper fractional SR Ca release curve (higher m) promotes alternans; 2), a smaller SR Ca uptake factor (lower u) promotes alternans, since alternans occurs at a lower value of m as u decreases; and 3,) a higher SR Ca leak (higher p) promotes alternans, since the threshold for m and u to reach the alternans region becomes lower if p is large (especially when u is small).

Validation by numerical simulations in a cardiac AP model

The iterated map model is explicitly constructed to allow the effects of the SR release slope, the SR Ca uptake factor, and the SR Ca leak factor to be varied independently, so that the dynamical contribution of each factor to the genesis of Ca_i alternans can be assessed independently of the other two factors. For example, the SR Ca leak factor can be increased in the map without altering the SR release slope or uptake factor. Physiologically, however, increased SR leak affects SR load, which secondarily affects the SR release slope and uptake, obscuring the independent contributions of each factor to the onset of Ca_i alternans. To establish the physiological relevance of the iterated map model, it is therefore essential to validate its predictions using a detailed cardiac AP model that inherently incorporates the interdependencies between SR Ca cycling components. In addition, only the detailed model allows direct comparison to myocyte experiments in which the same interdependencies are always present.

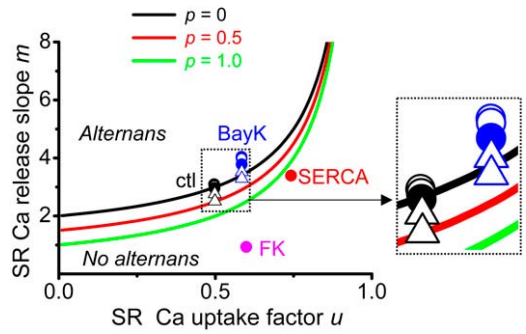

FIGURE 2 Iterated map prediction of Ca_i cycling stability. Plot of SR Ca release slope (m) versus SR Ca uptake factor (u) for different values of SR Ca leak factor (p) from the equation $(m+p-1)(1-u) = 1$, showing the boundaries separating the regions in which the Ca_i transient does or does not exhibit alternans. Black, red, and green curves correspond to the respective boundaries for increasing values of p (0, 0.5, and 1.0), illustrating that the greater the SR leak, the lower the threshold for the m and u parameters to produce alternans. Symbols represent the calculated values of m, p, and u from the AP model for control conditions (*black symbols*) and simulated effects of BayK (*blue symbols*), Ad-SERCA2a transfection (SERCA, *red symbols*), and FK506 (*purple symbols*) at different pacing CL, as described in the text. The inset shows a blow-up of the region for control conditions and BayK.

Using a detailed, physiologically realistic rabbit ventricular AP model (20), it is possible to calculate the values of m, u, and p (up to the point of the onset of Ca_i alternans to avoid violating the map assumption that total Ca t remains constant; see Appendix) for various parameter settings (see Methods). For control parameter settings during pacing with a fixed AP waveform, the onset of Ca alternans occurred at a pacing CL of 292 ms (Fig. 3 *A*, *black traces*). The calculated values of m, u, and p during steady-state pacing at this CL (see Methods) were 3.04, 0.497, and 0.067, respectively. This point (*solid black circle*) falls very near the stability boundary (*black line*) predicted by the iterated map in Fig. 2. Values of m, u, and p at slightly longer pacing CLs of 293 and 294 ms (*open black triangles*) fell slightly below this point toward the region of no alternans, whereas values at slightly shorter pacing CLs of 290 and 291 ms (*open black circles*) moved upward toward

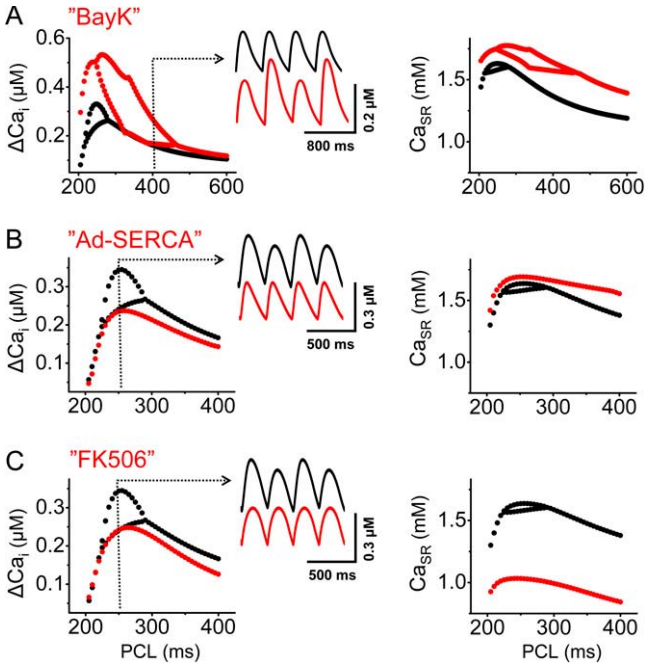

FIGURE 3 Ca_i alternans in the AP model. (*A*) Ca_i transient amplitude (*left*) and free SR Ca content (*right*) versus pacing cycle length (PCL) under control conditions (*black*) and after increasing the L-type Ca current conductance by a factor of two (*red*) to approximate the effects of BayK. Insets show Ca_i transients under both conditions at the PCL indicated by the dashed line. (*B* and *C*) Same as *A*, except red traces show simulation of either Ad-SERCA overexpression by increasing SERCA function (*B*) or FK506 by increasing SR Ca leak (*C*). In all cases, the AP model was paced using the same control AP waveform, according to the same dynamic pacing protocol used in myocyte experiments.

the region of alternans (see *inset*). Thus, for the control parameter settings, the iterated map accurately predicted the onset of Ca_i transient alternans during pacing with a constant AP waveform.

Fig. 3 *A* (*red traces*) shows the effect of increasing the maximum conductance of the L-type Ca current ($\bar{G}_{Ca}$) by 200% in the AP model. This caused the onset of Ca_i alternans to occur at a longer pacing CL (473 ms). The calculated values of m, u, and p at the onset of alternans were 3.78, 0.5843, and 0.11, respectively, which falls close to the stability boundary line predicted by the iterated map (*solid blue dot* in Fig. 2). This point moved downward toward the nonalternans region during pacing at longer CLs of 474 and 475 ms (*open blue triangles*, see *inset*) and upward toward the alternans region at shorter pacing CLs of 471 and 472 ms (*open blue circles*, see *inset*). The increased value of m at the onset of alternans compared to control conditions was due to the larger L-type Ca current triggering greater SR Ca release at a given SR Ca load (rather than increased SR Ca loading by the larger Ca current). Indeed, the SR Ca load at the onset of alternans was slightly lower compared to that under control conditions (92 vs. 95 μM, Fig. 3 *A*, *right panel*). u and p were also modestly increased at the onset of alternans. The increase in u is related to a greater fraction of SR Ca released by the larger L-type Ca current. The larger systolic Ca_i transient stimulates greater SR Ca uptake to restore the SR Ca content. The increase in p is related to the longer CL at the onset of Ca_i alternans, prolonging the diastolic interval during which the majority of SR Ca leak occurs.

Fig. 3 *B* (*red traces*) shows the effects doubling the maximum SR Ca uptake rate (v_{up}). During pacing with the same AP waveform, Ca_i alternans did not occur, even at the shortest pacing CL of 150 ms. The predominant effect of this intervention was to increase u, but m also increased due to increased SR filling. p was not significantly affected. At the same pacing CL of 292 ms that first induced alternans for the control parameter settings, the calculated values of m, u, and p changed from 3.04, 0.4969, and 0.067 to 3.39, 0.741, and 0.066, respectively. Even though the value of m increased, u also increased, so that this point (*solid red circle*) remained below the stability boundary line in the nonalternans region of the iterated map (Fig. 2).

Fig. 3 *C* (*red traces*) shows the effects of increasing SR Ca leak (g_l) by a factor of 20. During pacing with the same AP waveform, Ca_i alternans did not occur, even at the shortest pacing CL of 150 ms. This intervention predominantly increased p but also markedly decreased m (due to the decreased SR Ca load) and modestly increased u (due to the elevated diastolic Ca_i). At the same pacing CL of 292 ms that first induced alternans for the control parameter settings, the calculated values of m, u, and p changed from 3.04, 0.4969, and 0.067 to 0.932, 0.575, and 0.33, respectively. The dramatic decrease in m due to the unloading of the SR pushed this point (*solid purple circle*) well below the stability boundary line (i.e., between the *black* and *red lines* for $p = 0.33$) into the nonalternating regime of the iterated map (Fig. 2).

These findings demonstrate that the iterated map predicts with reasonable (but not perfect; see Discussion) accuracy the onset of Ca_i alternans in a realistic cardiac AP model during pacing with an AP clamp waveform under a variety of conditions with altered Ca_i cycling.

Comparison with experimental findings in isolated rabbit ventricular myocytes

We next compared the theoretical results with experimental data obtained from isolated rabbit ventricular myocytes loaded with Fluo-4AM or Rhod-2AM. Ca_i transients were measured at 34°C–36°C during pacing with an AP clamp waveform using the perforated patch configuration to minimize perturbation of the intracellular milieu. Using the identical dynamic pacing AP clamp protocol as in the numerical simulations, the onset of Ca_i alternans in the control group occurred at an average pacing CL of 226 $\pm$ 10 ms in 15 of 17 myocytes. In two myocytes, no Ca_i alternans developed even at the minimum pacing CL of 150 ms (the APD of the AP clamp). A representative example is shown in Fig. 4.

To increase SR Ca release slope in a manner approximating the AP simulations in Fig. 3 *A*, we superfused myo-

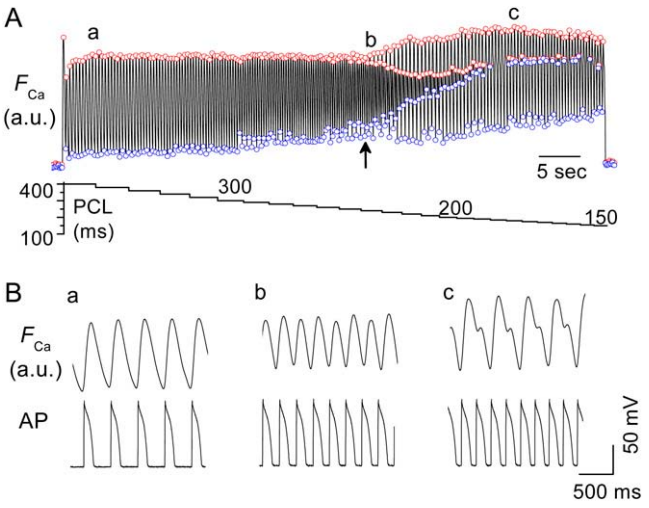

FIGURE 4 Ca_i alternans elicited by rapid pacing with an AP clamp in a representative isolated rabbit ventricular myocyte. (*A*) Ca_i fluorescence (F_{Ca}, *upper trace*) elicited by a clamped AP waveform (APD 150 ms) as the pacing cycle length (PCL, *lower trace*) was progressively decreased from 400 to 150 ms. Open dots show the diastolic (*blue*) and peak systolic (*red*) values of F_{Ca} during each beat, and the arrow indicates the onset of Ca_i alternans. (*B*) Expanded traces of F_{Ca} (*above*) and the AP waveform (*below*) at time points *a*–*c* in *A*. Note that in trace *c*, the small bump is a Ca_i transient elicited by the alternate AP clamps, reflecting severe Ca_i alternans.

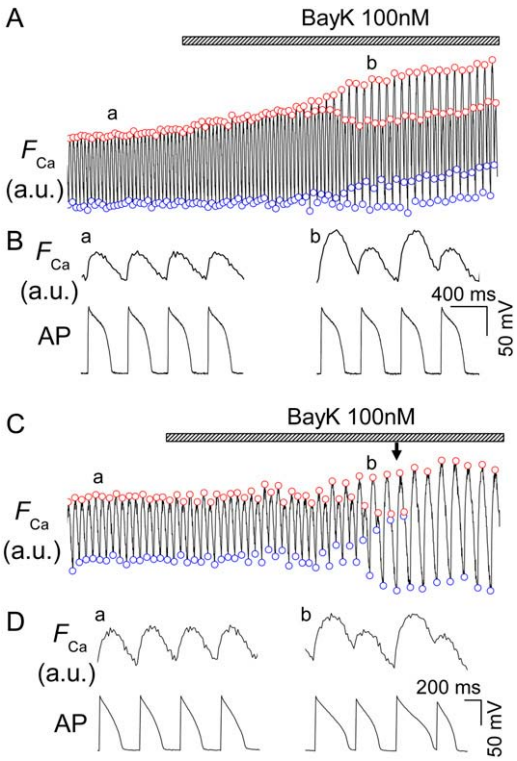

FIGURE 5 Effects of BayK on Ca_i alternans in isolated rabbit ventricular myocytes. (*A*) Ca_i fluorescence (F_{Ca}) during pacing at 400 ms with an AP clamp waveform (APD 150 ms) under control conditions and during application of 100 nM BayK (*horizontal bar*). Open dots show the diastolic (*blue*) and peak systolic (*red*) values of F_{Ca} during each beat, illustrating the onset of Ca_i alternans during BayK. (*B*) Expanded traces of F_{Ca} (*above*) and the AP clamp waveform (*below*) at time points *a* and *b* in *A*. (*C* and *D*) Same as *A* and *B* except with a free-running AP (current clamp mode) during pacing at 400 ms. Note in *D* that AP alternates concomitantly with Ca_i until, finally, a 2:1 block occurs (*arrow*).

cytes with the L-type Ca channel agonist BayK (100 nM). After BayK, the onset of Ca alternans during pacing with an AP clamp occurred at a much longer pacing CL (408 ± 15 ms, $n = 4$). Fig. 5 *A* shows a representative example. Before BayK, Ca_i alternans was absent in this myocyte during pacing with an AP clamp at CL 400 ms. The addition of BayK increased the Ca_i transient amplitude and induced Ca_i alternans at the same pacing CL. To corroborate whether BayK had increased the SR Ca release slope *m*, as predicted by the AP model, we compared Ca_i transients induced by rapid application of 10 mM caffeine in myocytes field stimulated at 1 Hz (to avoid Ca_i alternans) before and after BayK. BayK increased the AP-induced Ca_i transient as in Fig. 5 but did not increase the caffeine-induced Ca_i transient. This observation indicates that by enhancing the L-type Ca current, BayK increased the SR release fraction irrespective of SR Ca load, consistent with increased SR Ca release slope *m*.

To demonstrate the effects of Ca_i alternans on APD alternans, Fig. 5 *B* shows the effects of 100 nM BayK in a representative myocyte under current clamp conditions (2 ms stimuli at 2 nA) to allow free-running APs and Ca_i transients to be recorded simultaneously. Before BayK, neither APD nor Ca_i alternans were present during pacing at CL 400 ms. BayK prolonged APD and increased Ca_i transient amplitude, inducing both APD and Ca_i alternans. The relationship between APD and Ca_i alternans was concordant, i.e., the large Ca_i transient was associated with the long APD and vice versa (positive APD-Ca_i coupling (24)). Eventually, APD became so long that 2:1 block occurred.

To increase SR Ca uptake rate in a manner approximating the AP simulations in Fig. 3 *B*, we overexpressed SERCA2a using an adenoviral construct (25,26). Functional confirmation of SERCA2a overexpression was indicated by a marked acceleration of the half-time of Ca_i removal to 105 ± 9 ms ($n = 10$), compared to 193 ± 5 ms ($n = 17$) in nontransfected ($n = 8$) or GFP-alone transfected ($n = 9$) myocytes during pacing at 400 ms with a fixed AP waveform. As shown in Fig. 6 and summarized in Fig. 8, myocytes overexpressing SERCA2a were less susceptible to Ca_i alternans than were control myocytes, with only two of nine myocytes developing Ca_i alternans before reaching the shortest pacing CL of 150 ms. In the two myocytes that developed Ca_i alternans, the CLs at onset were 200 and 150 ms, respectively, compared to 226 ± 10 ms under control conditions ($p < 0.05$).

To increase SR Ca leak in a manner approximating the AP simulations in Fig. 3 *C*, we applied either ryanodine (1 μM) or FK506 (20 μM). As illustrated in Fig. 7 and summarized in Fig. 8, both drugs decreased susceptibility to alternans. Fig. 7 shows the effect of 20 μM FK506 in a representative myocyte. Before FK506, Ca_i alternans was present during pacing

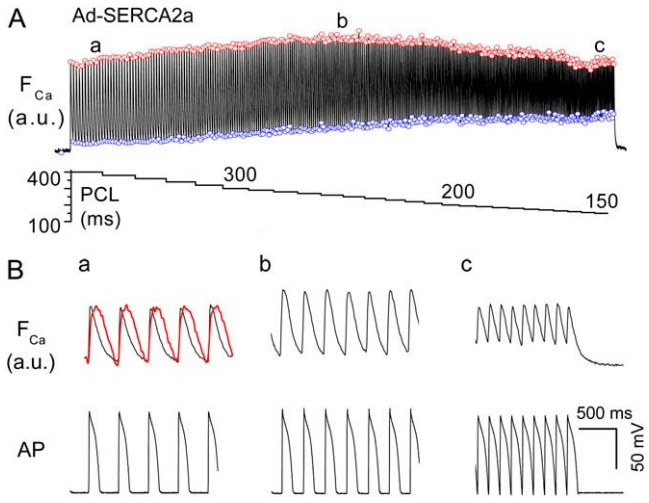

FIGURE 6 Effects of Ad-SERCA2a overexpression on Ca_i alternans. (*A*) Ca_i fluorescence (F_{Ca}, *upper trace*) elicited by a clamped AP waveform (APD 150 ms) as the pacing cycle length (PCL, *lower trace*) was progressively decreased from 400 to 150 ms, as in Fig. 4. Open dots show the diastolic (*blue*) and peak systolic (*red*) values of F_{Ca} during each beat. Ca_i alternans did not develop even at the shortest PCL. (*B*) Expanded traces of F_{Ca} (*above*) and the AP waveform (*below*) at time points *a–c* in *A*. The red trace in the left-hand panel is the superimposed Ca_i transient of a non-transfected myocyte at the PCL 400 ms, illustrating faster Ca_i removal in the Ad-SERCA2a-transfected myocyte.

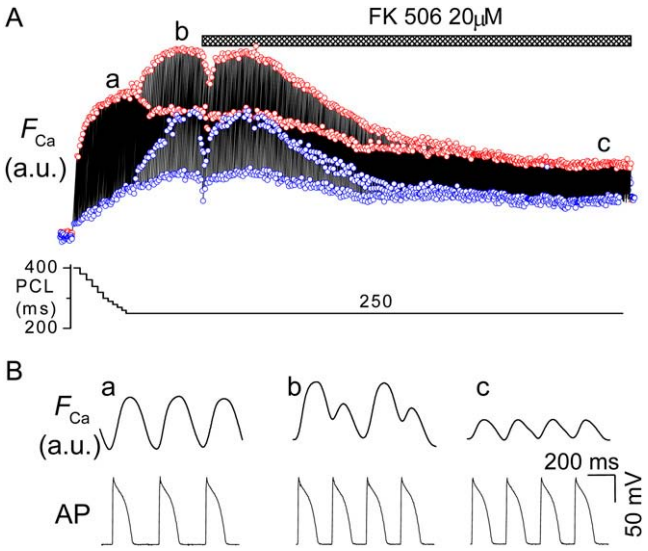

FIGURE 7 Effects of FK506 on Ca_i alternans. (*A*) Ca_i fluorescence (F_{Ca}, *upper trace*) elicited by a clamped AP waveform (APD 150 ms) as the pacing cycle length (PCL, *lower trace*) was progressively decreased from 400 to 250 ms and then held constant at 250 ms as FK506 (20 μM) was applied (*horizontal bar*). Open dots show the diastolic (*blue*) and peak systolic (*red*) values of F_{Ca} during each beat. As FK506 progressively decreased the peak F_{Ca}, Ca_i alternans was suppressed. (*B*) Expanded traces of F_{Ca} (*above*) and the AP waveform (*below*) at time points *a–c* in *A*.

with an AP clamp at a CL of 250 ms. The addition of FK506 suppressed Ca_i transient amplitude and abolished alternans, despite an increase in diastolic Ca_i.

These findings indicate that experimental data obtained from isolated rabbit ventricular myocytes agree well with the predictions from the iterated map and numerical simulations.

DISCUSSION

Pulsus alternans is a well-known sign of advanced heart failure, and electrocardiographic microvolt T wave alternans predicts increased arrhythmia risk in patients with diseased hearts (27). It is well accepted that T wave alternans arises from APD alternans at the cellular level. Two major factors known to promote APD alternans are steep APD restitution slope and Ca_i alternans. Because membrane voltage and Ca_i cycling are bidirectionally coupled, alternans in APD will cause the Ca_i transient to alternate and vice versa. Recent evidence, however, indicates that it is generally the Ca_i cycling instability that develops first as heart rate increases, since APD restitution slope is generally considerably <1 at the onset of APD alternans (1,2). Also, the susceptibility of ventricular endocardium versus epicardium to APD alternans correlates with differences in Ca_i cycling features but not APD restitution slope (2). Given the importance of repolarization alternans and pulsus alternans as poor prognostic signs in the failing heart, it is important to understand their cellular basis in relation to the excitation-contraction coupling defects promoted by heart failure.

In this study, we applied an iterated map approach to analyze the roles of the SR Ca release, uptake, and leak in regulating the onset of Ca_i alternans. Each factor was represented by a phenomenological parameter: m, the SR Ca release slope; u, the SR Ca uptake rate factor; and p, the SR Ca leak factor that could be independently varied without affecting the other parameters to isolate its dynamical role in Ca_i alternans. We first compared the map predictions to numerical simulations in a physiologically realistic cardiac AP model. Although m, u, or p could not be independently altered in the AP model without affecting each other, we could calculate their values under control conditions and after perturbing various aspects of Ca_i cycling to simulate (approximately) a series of experimentally testable interventions in isolated patch-clamped rabbit ventricular myocytes. Both the AP model and myocyte experiments showed good overall agreement with the map predictions, indicating that SR Ca release, uptake, and leak have independent direct effects that interact to regulate the onset of Ca_i alternans in cardiac myocytes. Our major conclusions are summarized below.

SR Ca release slope *m*

The map analysis predicts that high values of m strongly promote alternans, analogous to the role that increased gain plays in promoting oscillations in electronic circuits. We tested this prediction by potentiating the L-type Ca current in the AP model or applying BayK in isolated myocytes. This intervention increased SR Ca release slope m directly by

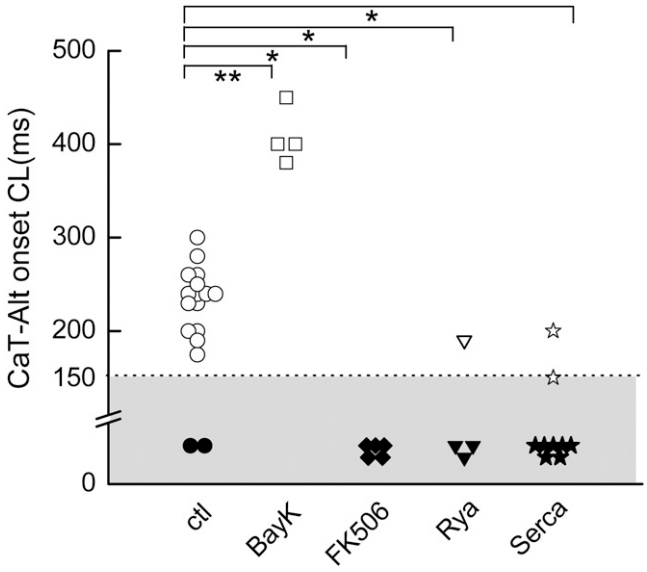

FIGURE 8 Summary of the effects of various interventions on Ca_i alternans. Scatter graph shows the pacing cycle length (PCL) at the onset of Ca_i alternans (CaT-Alt Onset CL) in rabbit ventricular myocytes during dynamic pacing with an AP clamp (APD 150 ms) under the following conditions: control, BayK (100 nM), FK506 (20 μM), ryanodine (Rya, 1 μM), and SERCA2a overexpression for 24–48 h (SERCA). Open symbols indicate myocytes that developed Ca_i alternans at the CL indicated; closed symbols in the gray area indicate myocytes that did not develop alternans down to the shortest PCL of 150 ms. * indicates $p < 0.05$ by Fisher's exact test, comparing the number of myocytes developing or not developing Ca_i alternans. ** indicates $p < 0.05$ by Student's *t*-test, comparing difference in CaT-Alt onset CL for the myocytes that developed alternans under control conditions versus BayK.

augmenting the trigger (the L-type Ca current) for any given SR Ca load. An indirect effect of increased SR Ca load on *m* did not appear to play a significant role, since the SR Ca load at the onset of Ca_i alternans was slightly lower after the L-type Ca current was potentiated to simulate the effects of BayK (Fig. 3 *A*). SR Ca uptake rate *u* and leak *p* were also increased modestly at the onset of alternans, reflecting the strong interdependency between all three SR Ca cycling factors. The net effect in both AP model and isolated myocytes was to cause Ca_i alternans to develop at a significantly longer pacing CL than under control conditions, as predicted by the map (Figs. 2 and 3 *A*). Intuitively, the mechanism can be understood as follows: irrespective of the SR Ca load, the increased L-type Ca current triggers the release of a greater fraction of SR Ca. To avoid alternans, the SR must then have the capacity to fully recover this greater amount of released Ca. Thus, unless SERCA2a function is also enhanced, Ca_i alternans will occur at a longer CL.

In the myocyte experiments, we could not directly measure the effects of BayK on the SR Ca load or the SR Ca release slope precisely at the onset of Ca_i alternans. Therefore, despite the general agreement with simulations, it is possible that nonspecific effects of BayK could have played a role. This caveat aside, our observations agree with prior experimental work demonstrating an important role of a steep SR Ca release slope in promoting Ca_i alternans (10,15). Moreover, our study extends their relevance to physiological temperature and rapid heart rates in the range relevant to clinical tachyarrhythmias, since the previous studies were performed at room temperature and used special voltage clamp conditions to induce CICR waves on alternate beats during relatively slow pacing. For Ca_i alternans induced by rapid pacing (CL $<$ 250 ms), however, it is not clear whether Ca waves will propagate rapidly enough to release a majority of the cell's SR Ca before the next depolarization (28). The important conclusion of this and prior theoretical studies (9,11,16), however, is that the temporal dynamics of SR Ca release slope, uptake, and leak are by themselves sufficient to explain rapid pacing-induced Ca_i alternans without the need to invoke the additional complexity of spatial factors such as subcellular Ca wave propagation.

For conceptual simplicity, we formulated the SR Ca release slope factor *m* in our map analysis as a direct function of SR Ca load (Fig. 1), in which case Ca_i alternans is always accompanied by alternans of the peak SR Ca load. A recent study (12), however, has shown that Ca_i alternans can occur without detectable alternans in peak SR Ca load, implying that, at the onset of Ca_i alternans, the state of RyR refractoriness is more important than peak SR Ca load in controlling SR Ca release. This interpretation is consistent with experimental data demonstrating that SR Ca refilling is faster than RyR recovery (29). The results of the map analysis are also consistent with this scenario, if *m* is redefined to represent SR Ca release as a function of RyR availability, rather than peak SR Ca load (the *x* axis of the *right-hand panels* in Fig. 1). In this case, the amplitude of the subsequent SR Ca release is a function of the greater (lesser) time required to refill the SR after a large (small) release, rather than the peak SR Ca load attained. For example, after a large SR Ca release, the greater depletion of SR Ca induces longer-lasting RyR refractoriness than after a small SR Ca release, even though peak SR Ca load recovers to the same level. At a molecular level, this could be due to either intrinsic Ca-dependent refractoriness properties of RyR or to slow binding-unbinding kinetics of calsequestran to junctin/triadin in the RyR complex (30).

SR Ca uptake rate *u*

High *u* strongly suppresses alternans, analogous to the role that shortening the feedback delay suppresses oscillations in electronic circuits. Intuitively, if *u* is high, then the SR can fully recover back to the same Ca load before the next AP arrives, ensuring that the AP will trigger the same amount of SR Ca release. When *u* is high, a very large value of *m* (gain factor) is required for alternans, but when *u* is low, a much smaller value of *m* induces instability. We tested this prediction by enhancing SR Ca uptake in the AP model. This intervention increased the value of *u* at any given pacing CL, and, despite increasing *m* by augmenting SR Ca load, still

suppressed alternans (Figs. 2 and 3 *B*). The value of *p* did not change. We evaluated the role of *u* experimentally by overexpressing SERCA2a in isolated myocytes. Previous studies with the identical vector documented a fivefold increase in protein expression and almost tripling of SR Ca content in isolated rabbit ventricular myocytes under similar conditions (25,26). Consistent with these findings, we observed that Ad-SERCA2a overexpression had a dramatic functional effect on accelerating the half-time of Ca_i removal. Consistent with the numerical simulations, Ad-SERCA2a overexpression dramatically suppressed Ca_i alternans, providing the first direct experimental evidence that increasing SR Ca uptake rate *u* suppresses Ca_i alternans under AP clamp conditions. A caveat is that we did not directly measure the effects of Ad-SERCA2a overexpression on SR Ca content in these myocytes. However, the alternative explanations for suppression of alternans, by Ad-SERCA2a overexpression either decreasing SR Ca content (and *m*) or by suppressing SR leak (and *p*), seem unlikely.

The map predicts, conversely, that decreasing *u* should promote alternans. This may explain why acute ischemia and heart failure promote Ca_i alternans (9,31), since both conditions suppress SERCA2a function—by ATP depletion and transcriptional downregulation, respectively. In contrast, β-adrenergic receptor stimulation both increases the L-type Ca current (like BayK) and enhances SR Ca uptake via SERCA2a. The first effect will promote Ca_i alternans by increasing *m*, whereas the second will suppress it by increasing *u*. This may explain why β-agonists and blockers have been reported to have variable effects in either suppressing or potentiating repolarization alternans (32–37) depending on which factor predominates under given experimental conditions.

SR Ca leak factor *p*

If *m* and *u* are unaffected (i.e., if the SR Ca load does not change), the pure direct effect of increased *p* is to promote alternans. Intuitively, this is because increased *p* effectively both enhances SR Ca release during systole (mimicking increased *m*) and slows SR Ca reuptake during diastole (mimicking decreased *u*). Its effect is strong when *u* is low and weak when *u* is high (Fig. 2). However, high *p* also decreases SR Ca load, which secondarily decreases *m*, suppressing alternans. The latter effect predominated in the AP model when SR Ca leak was directly enhanced (Figs. 2 and 3 *B*). Consistent with this prediction, when isolated myocytes were exposed to ryanodine or FK506 to enhance SR Ca leak indirectly by increasing the Ca sensitivity of RyR, Ca_i alternans was also suppressed. The converse effect may explain why tetracaine, which decreases SR Ca leak by directly blocking RyR but thereby indirectly enhances SR Ca load, was found to promote, rather than suppress, alternans (15). On the other hand, Lehnart et al. (19) reported that FKBP12.6-deficient mice, which demonstrate increased SR Ca leak, are more susceptible to APD alternans.

If APD alternans is in fact driven by Ca_i alternans in FKBP12.6-deficient mice, then this finding may indicate that in mice the SR Ca load is less depleted by increased SR leak, allowing the direct alternans-promoting effect of increased SR leak to become manifest. A limitation of our AP model is that it does not contain an explicit Markovian formulation of RyR required for simulating the molecular actions of FK506 and ryanodine directly (unfortunately, none of the existing AP models with Markovian RyR formulations exhibit Ca_i alternans). As these agents also affect other properties such as RyR Ca release sensitivity in addition to passive leak, their effects are not fully represented in our AP model. However, for these agents to suppress Ca_i alternans by a mechanism other than SR depletion, they would have to either reduce RyR Ca sensitivity (to decrease *m*) or enhance SR Ca uptake (to increase *u*). In contrast, ryanodine and FK506 both tend to increase RyR Ca sensitivity, and neither agent is known to directly enhance SERCA2a.

During heart failure, increased RyR leakiness combined with decreased SERCA2a expression may conspire to promote alternans by both increasing *p* and decreasing *u* (which amplifies the alternans-promoting effect of increased SR leak). In addition, Shannon et al. (38) have shown that SR Ca release slope *m* increases at low SR Ca loads in a rabbit heart failure model. These combined effects may all contribute to the increased susceptibility of the failing heart to Ca_i alternans.

Influence of Ca_i alternans on APD alternans

To analyze mechanisms of Ca_i alternans, we performed most simulations and experiments in the AP clamp mode to prevent APD alternans from affecting Ca_i alternans. Under physiological conditions in the beating heart, however, the onset of APD alternans is influenced by voltage-dependent factors such as APD restitution slope as well as Ca_i alternans (24), since Ca_i and APD are bidirectionally coupled. The coupling between Ca_i and APD is primarily determined by whether a large Ca_i transient promotes a net increase (via electrogenic Na-Ca exchange) or decrease (via accelerated inactivation of the L-type Ca current) in inward current during the AP plateau. If the Na-Ca exchange current effect dominates so that coupling between Ca_i and APD is positive (i.e., a larger Ca_i transient promotes a longer APD and vice versa), then voltage- and Ca_i-dependent factors will act synergistically to promote APD alternans at a slower pacing rate than would otherwise be required for either factor alone to induce alternans.

In this case, APD and Ca_i alternans are electromechanically concordant, i.e., the long APD is associated with the large Ca_i transient and vice versa. On the other hand, theoretical analysis shows that if the coupling between APD and Ca_i is negative, a faster pacing rate will be required to induce alternans, and APD and Ca_i alternans may be electromechanically concordant, discordant, or vary quasiperiodically

(24). Electromechanically discordant and quasiperiodically varying alternans have been observed in other species and experimental conditions (39–41), but we did not observe this behavior in rabbit ventricular myocytes under any of our experimental conditions. However, it remains possible that interventions influencing m, u, or p could change the sign of Ca_i-APD coupling by altering the relative influences of Na-Ca exchange versus L-type Ca current inactivation on APD.

Limitations

Like any mathematical formulation, the iterated map approach is limited by the accuracy of its assumptions. In particular, formulating the Ca_i transient of the current beat solely as a function of the previous beat does not take into account the possible influence of even earlier beats. In the AP model, these pacing history (memory) influences are likely to account for the minor discrepancies between the stability boundary locations on the map and the slightly offset positions of points calculated from the AP model in Fig. 2. In real cells, other factors not incorporated into the AP model, such as mitochondrial and nuclear Ca sequestration/release and protein kinase/phosphatase regulation of Ca_i cycling elements, are also likely to operate over a timescale of many beats. Some of the drugs used, such as BayK and FK506, may have complex or nonselective effects. Despite these limitations, the agreement between the iterated map predictions and both the numerical AP simulations and experimental findings in isolated myocytes is reasonably close, suggesting that the fundamental dynamics, if not all the details, are accurately captured by the map.

APPENDIX

The iterated map formulation summarizes how the Ca_i transient amplitude and SR Ca_i release, reuptake, and leak during the previous beat determine the values of the same parameters during the current beat. We define l_n as the SR Ca load at the start of the nth beat and r_n as the amount of SR Ca released during the nth beat. From the nonlinear curve relating fractional SR Ca release to SR Ca load (Fig. 1), we can predict that very close to the onset of Ca_i alternans during the nth beat, the change in SR Ca release ($\Delta r_n = r_n - r_{eq}$) relative to the equilibrium value r_{eq} is proportional to the change in SR Ca load ($\Delta l_n = l_n - l_{eq}$), i.e.,

$$\Delta r_n = m\Delta l_n, \tag{1}$$

where m is the slope of the fractional SR Ca release curve at the equilibrium value of the SR load l_{eq} (i.e., the slope of the *curve* in Fig. 1), assuming that the nth beat is very close to the equilibrium (i.e., linear approximation). The Ca in the cytoplasm after SR Ca release occurs on the nth beat will be the amount in the cytoplasm before release ($t - l_n$) plus the amount released (r_n):

$$t - l_n + r_n, \tag{2}$$

where t, the total Ca in the myocyte, is assumed to be constant at the onset of Ca_i alternans. After SR Ca release on the nth beat, the amount of Ca left in the SR for the next beat, l_{n+1}, will be the starting SR load of the nth beat (l_n), less the SR leak (pl_n) during the nth beat, less the amount released during the nth beat (r_n), plus the amount of released Ca pumped back into the SR by the SERCA2a Ca pump, i.e.,

$$l_{n+1} = l_n - pl_n - r_n + u(t - l_n - pl_n + r_n). \tag{3}$$

Note that right at the onset of alternans, the total Ca t is assumed to be constant, i.e., the amount of Ca influx via the L-type Ca current is exactly balanced by the Ca efflux via the Na-Ca exchanger, so that these terms cancel each other and do not need to be explicitly included in Eq. 3. Also note that here, unlike previous formulations (9,11,16), we have explicitly incorporated the term p for SR Ca leak, whose value is proportional to the SR Ca content l_n during the nth beat. We assume that the SR Ca leak during the nth beat does not contribute significantly to the cytosolic Ca_i transient of the nth beat, since most of the SR Ca leak occurs during diastole following the Ca_i transient as the SR refills. The net amount of Ca pumped back up into the SR is given by the last term, $u(t - l_n(1 - p) + r_n)$, where u is defined as the SR Ca uptake factor reflecting Ca resequestration via SERCA2a. This term includes the leak factor p during the nth beat, since the SR Ca leak occurs predominantly during diastole as the SR Ca content increases. At equilibrium, Eq. 3 is still valid, i.e.,

$$l_{eq} = l_{eq}(1 - p) - r_{eq} + u(t - l_{eq}(1 - p) + r_{eq}); \tag{4}$$

so subtracting Eq. 4 from Eq. 3, we then have

$$\begin{aligned} \Delta l_{n+1} &= \Delta l_n(1 - p) - \Delta r_n + u(-\Delta l_n(1 - p) + \Delta r_n) \\ \Delta l_{n+1} &= (1 - p)(1 - u)\Delta l_n - (1 - u)\Delta r_n \end{aligned} \tag{5}$$

where $\Delta l_n = l_n - l_{eq}$. Substituting Eq. 1 into Eq. 5, we obtain

$$\Delta l_{n+1} = -\frac{(m + p - 1)(1 - u)}{m}\Delta r_n \tag{6}$$

The stability criteria predicting for the onset of Ca_i alternans can be derived by substituting Eq. 1 into Eq. 6, i.e.,

$$\Delta l_{n+1} = -(m + p - 1)(1 - u)\Delta l_n, \tag{7}$$

which by iteration gives

$$\Delta l_n = \Delta l_0[-(m + p - 1)(1 - u)]^n. \tag{8}$$

Equation 8 predicts that the onset of Ca_i alternans occurs when the quantity in brackets raised to the nth power is <-1, i.e., $-(m+p-1)(1-u) < -1$ or $(m+p-1)(1-u) > 1$, which is the condition for the magnitude of the SR load perturbation Δl_n to grow exponentially with increasing beat number and for the sign of Δl_n to alternate from beat to beat.

We thank Federica Del Monte for kindly providing the Ad-SERCA2a-GFP construct, Yohannes Shiferaw and Alain Karma for helpful discussions, Ming-Jim Yang for data statistics, and Tan Duong for superb technical support.

The study was supported by National Institutes of Health/National Heart, Lung, and Blood Institute grants P50 HL53219 and P01 HL078931 and Laubisch and Kawata endowments.

REFERENCES

1. Chudin, E., J. Goldhaber, A. Garfinkel, J. Weiss, and B. Kogan. 1999. Intracellular Ca^{2+} dynamics and the stability of ventricular tachycardia. *Biophys. J.* 77:2930–2941.
2. Pruvot, E. J., R. P. Katra, D. S. Rosenbaum, and K. R. Laurita. 2004. Role of calcium cycling versus restitution in the mechanism of repolarization alternans. *Circ. Res.* 94:1083–1090.
3. Pruvot, E., R. P. Katra, D. S. Rosenbaum, and K. R. Laurita. 2002. Calcium cycling as mechanism of repolarization alternans onset in the intact heart. *Circulation.* 106:191–192.
4. Goldhaber, J. I., L. H. Xie, T. Duong, C. Motter, K. Khuu, and J. N. Weiss. 2005. Action potential duration restitution and alternans in

rabbit ventricular myocytes: the key role of intracellular calcium cycling. *Circ. Res.* 96:459–466.

5. Pastore, J. M., S. D. Girouard, K. R. Laurita, F. G. Akar, and D. S. Rosenbaum. 1999. Mechanism linking T-wave alternans to the genesis of cardiac fibrillation. *Circulation.* 99:1385–1394.
6. Cao, J. M., Z. Qu, Y. H. Kim, T. J. Wu, A. Garfinkel, J. N. Weiss, H. S. Karagueuzian, and P. S. Chen. 1999. Spatiotemporal heterogeneity in the induction of ventricular fibrillation by rapid pacing: importance of cardiac restitution properties. *Circ. Res.* 84:1318–1331.
7. Qu, Z. L., A. Garfinkel, P. S. Chen, and J. N. Weiss. 2000. Mechanisms of discordant alternans and induction of reentry in simulated cardiac tissue. *Circulation.* 102:1664–1670.
8. Watanabe, M. A., F. H. Fenton, S. J. Evans, H. M. Hastings, and A. Karma. 2001. Mechanisms for discordant alternans. *J. Cardiovasc. Electrophysiol.* 12:196–206.
9. Weiss, J. N., A. Karma, Y. Shiferaw, P. S. Chen, A. Garfinkel, and Z. Qu. 2006. From pulsus to pulseless: the saga of cardiac alternans. *Circ. Res.* 98:1244–1253.
10. Diaz, M. E., S. C. O'Neill, and D. A. Eisner. 2004. Sarcoplasmic reticulum calcium content fluctuation is the key to cardiac alternans. *Circ. Res.* 94:650–656.
11. Shiferaw, Y., M. Watanabe, A. Garfinkel, J. Weiss, and A. Karma. 2003. Model of intracellular calcium cycling in ventricular myocytes. *Biophys. J.* 85:3666–3686.
12. Picht, E., J. Desantiago, L. A. Blatter, and D. M. Bers. 2006. Cardiac alternans do not rely on diastolic sarcoplasmic reticulum calcium content fluctuations. *Circ. Res.* 99:740–748.
13. Bassani, J. W., W. Yuan, and D. M. Bers. 1995. Fractional SR Ca release is regulated by trigger Ca and SR Ca content in cardiac myocytes. *Am. J. Physiol. Cell Physiol.* 268:C1313–C1319.
14. Shannon, T. R., K. S. Ginsburg, and D. M. Bers. 2000. Potentiation of fractional sarcoplasmic reticulum calcium release by total and free intra-sarcoplasmic reticulum calcium concentration. *Biophys. J.* 78: 334–343.
15. Diaz, M. E., D. A. Eisner, and S. C. O'Neill. 2002. Depressed ryanodine receptor activity increases variability and duration of the systolic Ca^{2+} transient in rat ventricular myocytes. *Circ. Res.* 91:585–593.
16. Qu, Z., Y. Shiferaw, and J. N. Weiss. 2007. Nonlinear dynamics of cardiac excitation-contraction coupling: an iterated map study. *Phys. Rev. E.* 75:011927.
17. Cutler, M. J., X. Wan, R. J. Hajjar, and D. S. Rosenbaum. 2007. Targeted SERCA2a gene overexpression identifies mechanism and potential therapy for arrhythmogenic cardiac alternans. *Circulation.* 116:II_217.
18. Wehrens, X. H., S. E. Lehnart, and A. R. Marks. 2005. Intracellular calcium release and cardiac disease. *Annu. Rev. Physiol.* 67:69–98.
19. Lehnart, S. E., C. Terrenoire, S. Reiken, X. H. Wehrens, L. S. Song, E. J. Tillman, S. Mancarella, J. Coromilas, W. J. Lederer, R. S. Kass, and A. R. Marks. 2006. Stabilization of cardiac ryanodine receptor prevents intracellular calcium leak and arrhythmias. *Proc. Natl. Acad. Sci. USA.* 103:7906–7910.
20. Mahajan, A., Y. Shiferaw, D. Sato, A. Baher, R. Olcese, L.-H. Xie, M.-J. Yang, P.-S. Chen, J. G. Restrepo, A. Karma, A. Garfinkel, Z. Qu, and J. N. Weiss. 2008. A rabbit ventricular action potential model replicating cardiac dynamics at rapid heart rates. *Biophys. J.* 94:392–410.
21. Nolasco, J. B., and R. W. Dahlen. 1968. A graphic method for the study of alternation in cardiac action potentials. *J. Appl. Physiol.* 25:191–196.
22. Goldhaber, J. I., J. M. Parker, and J. N. Weiss. 1991. Mechanisms of excitation-contraction coupling failure during metabolic inhibition in guinea-pig ventricular myocytes. *J. Physiol.* 443:371–386.
23. Rae, J., K. Cooper, P. Gates, and M. Watsky. 1991. Low access resistance perforated patch recordings using amphotericin B. *J. Neurosci. Methods.* 37:15–26.
24. Shiferaw, Y., D. Sato, and A. Karma. 2005. Coupled dynamics of voltage and calcium in paced cardiac cells. *Phys. Rev. E.* 71:021903.
25. Davia, K., E. Bernobich, H. K. Ranu, F. del Monte, C. M. Terracciano, K. T. MacLeod, D. L. Adamson, B. Chaudhri, R. J. Hajjar, and S. E. Harding. 2001. SERCA2A overexpression decreases the incidence of aftercontractions in adult rabbit ventricular myocytes. *J. Mol. Cell. Cardiol.* 33:1005–1015.
26. Terracciano, C. M., R. J. Hajjar, and S. E. Harding. 2002. Overexpression of SERCA2a accelerates repolarisation in rabbit ventricular myocytes. *Cell Calcium.* 31:299–305.
27. Rosenbaum, D. S., L. E. Jackson, J. M. Smith, H. Garan, J. N. Ruskin, and R. J. Cohen. 1994. Electrical alternans and vulnerability to ventricular arrhythmias. *N. Engl. J. Med.* 330:235–241.
28. Miura, M., P. A. Boyden, and H. E. ter Keurs. 1999. Ca^{2+} waves during triggered propagated contractions in intact trabeculae. Determinants of the velocity of propagation. *Circ. Res.* 84:1459–1468.
29. Brochet, D. X., D. Yang, A. Di Maio, W. J. Lederer, C. Franzini-Armstrong, and H. Cheng. 2005. Ca^{2+} blinks: rapid nanoscopic store calcium signaling. *Proc. Natl. Acad. Sci. USA.* 102:3099–3104.
30. Gyorke, I., N. Hester, L. R. Jones, and S. Gyorke. 2004. The role of calsequestrin, triadin, and junctin in conferring cardiac ryanodine receptor responsiveness to luminal calcium. *Biophys. J.* 86:2121–2128.
31. Taggart, P., P. M. Sutton, M. R. Boyett, M. Lab, and H. Swanton. 1996. Human ventricular action potential duration during short and long cycles. Rapid modulation by ischemia. *Circulation.* 94:2526–2534.
32. Nearing, B. D., A. H. Huang, and R. L. Verrier. 1991. Dynamic tracking of cardiac vulnerability by complex demodulation of the T wave. *Science.* 252:437–440.
33. Euler, D. E., H. Guo, and B. Olshansky. 1996. Sympathetic influences on electrical and mechanical alternans in the canine heart. *Cardiovasc. Res.* 32:854–860.
34. Dumitrescu, C., P. Narayan, I. R. Efimov, Y. Cheng, M. J. Radin, S. A. McCune, and R. A. Altschuld. 2002. Mechanical alternans and restitution in failing SHHF rat left ventricles. *Am. J. Physiol. Heart Circ. Physiol.* 282:H1320–H1326.
35. Rashba, E. J., M. Cooklin, K. MacMurdy, N. Kavesh, M. Kirk, S. Sarang, R. W. Peters, S. R. Shorofsky, and M. R. Gold. 2002. Effects of selective autonomic blockade on T-wave alternans in humans. *Circulation.* 105:837–842.
36. Kameyama, M., Y. Hirayama, H. Saitoh, M. Maruyama, H. Atarashi, and T. Takano. 2003. Possible contribution of the sarcoplasmic reticulum Ca^{2+} pump function to electrical and mechanical alternans. *J. Electrocardiol.* 36:125–135.
37. Taggart, P., P. Sutton, Z. Chalabi, M. R. Boyett, R. Simon, D. Elliott, and J. S. Gill. 2003. Effect of adrenergic stimulation on action potential duration restitution in humans. *Circulation.* 107:285–289.
38. Shannon, T. R., F. Wang, and D. M. Bers. 2005. Regulation of cardiac sarcoplasmic reticulum Ca release by luminal [Ca] and altered gating assessed with a mathematical model. *Biophys. J.* 89:4096–4110.
39. Murphy, C. F., S. M. Horner, D. J. Dick, B. Coen, and M. J. Lab. 1996. Electrical alternans and the onset of rate-induced pulsus alternans during acute regional ischaemia in the anaesthetised pig heart. *Cardiovasc. Res.* 32:138–147.
40. Otani, N. F., and R. F. Gilmour Jr. 1997. Memory models for the electrical properties of local cardiac systems. *J. Theor. Biol.* 187:409–436.
41. Gilmour, R. F., N. F. Otani, and M. A. Watanabe. 1997. Memory and complex dynamics in cardiac Purkinje fibers. *Am. J. Physiol. Heart Circ. Physiol.* 41:H1826–H1832.